# Flow impingement onto a flat plate with limited heated area in relation to laser gas assisted processing

## Influence of nozzle geometry on heat transfer rates

Received June 2003
Revised March 2004
Accepted June 2004

S.Z. Shuja, B.S. Yilbas and M.O. Budair
*Department of Mechanical Engineering, KFUPM, Dhahran, Saudi Arabia*

### Abstract

**Purpose** – To investigate the influence of conical and annular nozzle geometric configurations on the flow structure and heat transfer characteristics near the stagnation point of a flat plate with limited heated area.

**Design/methodology/approach** – The conical and annular conical nozzles were designed such that the exit area of both nozzles is the same and the mass flow rate passing through the nozzles is kept constant for both nozzles. The governing equations of flow and heat transfer are modeled numerically using a control volume approach. The grid independent solutions are secured and the predictions of flow and heat transfer characteristics are compared with the simple pipe flow with the same area and mass flow rate. The Reynolds stress turbulence model is employed to account for the turbulence. A flat plate with a limited heated area is accommodated to resemble the laser heating situations and air is used as assisting gas.

**Findings** – It is found that nozzle exiting velocity profiles differ considerably with changing the nozzle cone angle. Increasing nozzle cone angle enhances the radial flow and extends the stagnation zone away from the plate surface. The impinging jet with a fully developed velocity profile results in enhanced radial acceleration of the flow. Moreover, the flow structure changes considerably for annular conical and conical nozzles. The nozzle exiting velocity profile results in improved heat transfer coefficient at the flat plate surface. However, the achievement of fully developed pipe flow like velocity profile emanating from a nozzle is almost impossible for practical laser applications. Therefore, use of annular conical nozzles facilitates the high cooling rates from the surface during laser heating process

**Research limitations/implications** – The results are limited with theoretical predictions due to the difficulties arising in experimental studies.

**Practical implications** – The results can be used in laser machining applications to improve the end product quality. It also enables selection of the appropriate nozzle geometry for a particular machining application.

**Originality/value** – This paper provides information on the flow and heat transfer characteristics associated with the nozzle geometric configurations and offers practical help for the researchers and scientists working in the laser machining area.

**Keywords** Flow measurement, Geometry, Lasers, Gas flow

**Paper type** Research paper

International Journal for Numerical Methods in Heat & Fluid Flow
Vol. 15 No. 4, 2005
pp. 363-378

0961-5539
DOI 10.1108/09615530510590614

## Nomenclature

$H$ = enthalpy
$K$ = thermal conductivity
$k$ = turbulent kinetic energy
$p$ = pressure
$P$ = rate of production
$R_{ij}$ = Reynolds stress
Re = Reynolds number
$r$ = distance in the radial direction
$t$ = time
$T$ = temperature
$u^*$ = friction velocity
$U$ = arbitrary velocity
$\forall$ = volume
$x$ = distance in the axial direction
$x_n$ = distance to the nearest wall
$x_{max}$ = distance to the solid rear surface

*Greek*

$\alpha$ = thermal diffusivity
$\Gamma$ = arbitrary diffusion coefficient
$\varepsilon$ = energy dissipation
$\lambda$ = turbulence intensity
$\mu$ = dynamic viscosity
$\nu$ = kinematic viscosity
$\rho$ = density (function of temperature and pressure for gas)
$\sigma$ = variable Prandtl no.
$\Phi$ = viscous dissipation
$\phi$ = arbitrary variable
$\Pi$ = energy transport due to pressure excluding strain interactions
$\Pi^w$ = energy transport due to wall reflection
$\Lambda$ = energy transport by diffusion

*Subscript*

amb = ambient
*i,j* = arbitrary direction
jet = gas jet at inlet
l = laminar
p = a typical node in the computational grid
t = turbulent
n,s,e,w,l,h = north, south, east, west, low or high node
w = wall

## 1. Introduction

Laser surface treatment process is involved with laser heating and gas assisting processes. In laser conduction limited heating situations, substrate material is heated up to the melting temperature of the substrate material. In this case, assisting gas is used to prevent high temperature oxidation reactions taking place at the substrate surface, i.e. material remains at about the melting temperature of the substrate material at the surface while assisting gas protects the surface from oxidation reactions. The assisting gas, in this case, is an inert gas such as argon, helium, and so on. In laser gas assisting processing, assisting gas impinges onto the substrate surface. Consequently, a convergent nozzle is used to discharge the assisting gas impinging onto the substrate surface. Depending on the nozzle geometric configurations, the velocity distribution of the assisting gas across the nozzle exit changes considerably; in an effect, it influences the heat transfer characteristics of the laser irradiated surface.

Considerable research studies were carried out to investigate the laser conduction limited heating process. Simon *et al.* (1993) studied the conduction losses during laser welding by time-modulated laser beam. They indicated that the oscillation in the laser pulse did not have a significant effect on the size of the heat affected zone. Neto and Lima (1994) numerically solved parabolic form of heat conduction equation due to laser pulse irradiation. They indicated that the solution obtained agreed well with the experimental results. Hector *et al.* (1992) developed an analytical formulation of the mode locked laser heating process. They assumed a surface heat source in modelling the heating process. They showed that parabolic heating model over-predicted the temperature during the short-pulse heating process. Yilbas and Shuja (1997)

investigated the conduction limited heating process due to laser pulse irradiation. They showed that temperature rise attained almost steady value as heating progressed. Yilbas (1997) studied analytically laser pulse heating process. He formulated the temperature rise during the heating pulse. Moreover, in general, the studies related to laser conduction limited heating situation is limited to non-convective boundary conditions at the surface. However, few studies were conducted to investigate the laser gas assisted processing (Shuja and Yilbas, 1998; Shuja *et al.*, 1998). It should be noted that in the previous study (Yilbas *et al.*, 2002), the assisting gas, which impinges onto the workpiece surface is assumed to be fully developed when exiting the nozzle. This assumption may not be true solely, since the nozzle exit flow situation differs than fully developed pipe flow exit conditions. Moreover, assisting gas cools the irradiated substrate surface convectively and the cooling rate of the surface depends on the heat transfer coefficient which becomes important when exceeding $10^7$ W/m$^2$ K (Yilbas *et al.*, 2000), i.e. heat transfer rates signify as the heat transfer coefficient exceeds $10^7$ W/m$^2$. In laser practical applications circular conical nozzles are used. However, heat transfer characteristics may possibly be improved using different nozzle configurations. Therefore, study into the influence of nozzle geometric configuration onto flow and heat transfer characteristics in laser gas assisted processing is necessary.

Considerable research studies were carried out to investigate the flow and heat transfer characteristics due to jet impingement onto surfaces. The local heat transfer coefficient distribution on a square source due to a normally impinging axisymmetric confined liquid jet was studied by Morris *et al.* (1996). They showed that the predictions agreed with the experimental results to within 16-20 per cent. They indicated that difference was due to the turbulence model employed which failed to predict the near-wall situation. Heat transfer measurements from a surface with uniform heat flux and an impinging jet were carried out by Baughn and Shimizu (1989). They indicated that the effect of jet distance (nozzle-to-plate spacing) on the stagnation point heat transfer was maximum when the jet distance becomes six times of the nozzle exit diameter. Impinging jet studies for turbulence model assessment were carried out by Cooper *et al.* (1993). They showed that $k$-$\varepsilon$ turbulence model over-predicted the kinetic energy generation in the region near to the stagnation zone. A local impingement heat transfer for a free surface due to turbulent water jet was investigated by Wolf *et al.* (1995a, b). They indicated that the velocity gradient along the impingement surface was insensitive to the Reynolds number and varied approximately linearly with the nozzle-to-surface spacing. A numerical study characterising the thermal behaviour of laminar circular liquid jets was carried out by Lee *et al.* (1995). They indicated that results exhibited good agreement with the experimental data, in which case, the significance of recovery effect with large Prandtl number liquid jets was verified. Fully developed liquid jets impinging on a constant heat flux surface were investigated by Elison and Webb (1994). They showed that the Nusselt number was independent of nozzle-to-plate spacing in the initially laminar jet regime. Heat transfer between a uniformly heated flat plate and impinging circular air jet was investigated by Huang and El-Genk (1994). They showed that the maximum Nusselt number was a strong function of nozzle-to-plate spacing. Mohanty and Tawfek (1993) studied heat transfer rates due to a round jet impingement onto a flat surface. They indicated that the heat transfer rate decayed exponentially with radial distance. The turbulent flow structure due to impinging axisymmetric liquid jets was studied by

Stevens *et al.* (1992a, b). They indicated that turbulence levels were to be strongly influenced by the nozzle exit conditions. Garimella and Rice (1995) investigated the heat transfer characteristics of impinging liquid jets. They observed the secondary peak in the local heat transfer coefficient in the radial direction and stated that the magnitude of secondary peak was increased with increasing Reynolds number. Shuja *et al.* (1999) investigated the flow and heat transfer characteristics due to impinging jet onto a limited area heated surface. They showed that low-Reynolds number turbulence model predicted the Nusselt number distribution in the radial direction correctly, i.e. predictions agreed well with the experimental results reported in the open literature.

In the present study, jet impingement onto a limited area heated flat plate is considered in relation to laser gas assisted conduction limited heating. The nozzle configuration of the jet are varied and heat transfer coefficient due to different nozzle configurations are computed. Annular-conical and conical nozzle types with different cone angles are employed in the simulations. The study is extended to include the fully developed jet, emerging from the pipe exit, impinging onto a flat surface. Reynolds stress turbulence model is employed to account for the turbulence.

## 2. Mathematical modelling

In laser gas assisted processing, the impinging jet conditions are mainly steady; consequently, steady-flow conditions are considered in the analysis, provided that the compressibility effect and variable properties are accommodated. The jet impinging onto a limited heated area flat plate is simulated. The wall temperature of the heated area is kept constant at 1,500 K to resemble the laser heating situation. The geometric arrangements of the annular conical and conical nozzles and the plate are shown in Figure 1 while nozzle configurations are given in Table I.

### *2.1 Flow equations*

The governing flow and energy equations for the axisymmetric impinging jet can be written in the Cartesian tensor notation as:

the continuity equation:

$$\frac{\partial}{\partial x_i}(\rho U_i) = 0 \tag{1}$$

the momentum equation:

$$\frac{\partial}{\partial x_i}(\rho U_i U_j) = -\frac{\partial p}{\partial x_j} + \frac{\partial}{\partial x_i}\left[\mu\left(\frac{\partial U_i}{\partial x_j} + \frac{\partial U_j}{\partial x_i}\right) - \rho R_{ij}\right] \tag{2}$$

the energy equation:

$$\frac{\partial}{\partial x_i}(\rho U_i H) = \frac{\partial}{\partial x_i}\left[\frac{\mu}{\sigma}\frac{\partial H}{\partial x_i} - \rho R_{i\mathrm{h}}\right] \tag{3}$$

when modelling the Reynolds stresses and turbulence properties following steps are considered.

*Reynolds stresses* ($R_{ij}$). The RSTM is based on the second-moment closure (Launder, 1989). The transport equation of the Reynolds stress ($R_{ij}$) is:

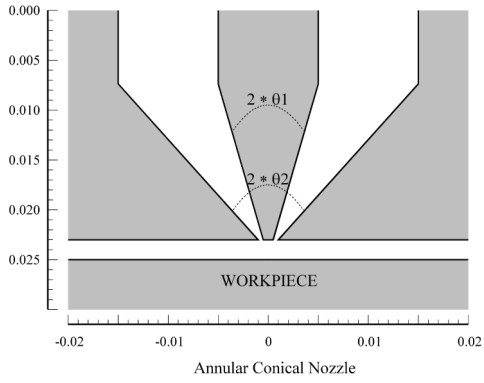


**Figure 1.**
Cross-sectional view of annular-conical and conical nozzles. $\theta 1$ and $\theta 2$ are inner and outer cone angles of the nozzles, respectively

| Nozzle no. | Annular nozzle Inner cone angle (°) | Annular nozzle Outer cone angle (°) | Conical nozzle Cone angle (°) |
|---|---|---|---|
| 1 | 25 | 55.42 | 55.42 |
| 2 | 30 | 60.89 | 60.89 |
| 3 | 35 | 65.34 | 65.34 |
| 4 | 40 | 69.04 | 69.04 |

**Table I.**
Geometry configuration of annular and conical nozzles

$$\frac{\partial}{\partial x_{\mathrm{m}}}(U_{\mathrm{m}}R_{ij}) = P_{ij} + \Lambda_{ij} - \varepsilon_{ij} + \Pi_{ij} + \Pi_{ij}^{\mathrm{w}} \tag{4}$$

where $P$, $\Lambda$, $\varepsilon$, $\Pi$ and $\Pi^{\mathrm{w}}$ are the rate of production, transport by diffusion, rate of dissipation, transport due to turbulent pressure excluding strain interactions and transport due to wall reflection, respectively. Equation (4) consists of six partial differential equations; one for the transport of each of the six independent Reynolds

stresses. The production term ($P_{ij}$), diffusion ($\Lambda_{ij}$), dissipation ($\varepsilon_{ij}$), transport due to turbulent pressure ($\Pi_{ij}$) and the modelling of the wall reflection $\left(\Pi_{ij}^{w}\right)$ are refereed in Launder (1989).

*2.2 Flow boundary conditions*

Four boundary conditions are considered in accordance with the geometric arrangement of the problem as shown in Figure 1; these are:

*Solid wall.* No slip condition is assumed at the solid wall and the boundary condition for the velocity at the solid wall is therefore:

$$U_{\mathrm{i}} = 0$$

*Generalized wall functions for normal and shear turbulent stresses for the RSTM model.* When the flow is very near the wall it undergoes a rapid change in direction, the wall-functions approach is not successful in reproducing the details of the flow. Consequently the turbulent stresses and fluxes at the near-wall grid points are calculated directly from their transport equations. In this case, the near-wall region lying between the wall and the near-wall computational node at $x_{\mathrm{p}}$ can be represented by two layers: the fully viscous sublayer, defined by $\mathrm{Re}_v = x_{\mathrm{v}}\sqrt{k_{\mathrm{v}}}/\nu \cong 20$, and a fully turbulent layer. The wall shear stress near the wall is employed, i.e. $\overline{vw}|_{z_{\mathrm{v}}} = \tau_{\mathrm{w}}/\rho$, which serves as the boundary condition for the $\overline{vw}$ transport equation.

In relation to normal stresses, the turbulence energy must decrease quadratically towards a value of zero at the wall (Benocci, 1991), therefore a zero-gradient condition for the normal stresses is physically realistic. This situation is insufficient to ensure an accurate numerical representation of near-wall effects. An improved approach for internal cells is needed in respect of evaluating volume-integrated production and dissipation of normal stresses (these are normally evaluated at cell centres, using linear interpolation, and then multiplied by the cell volume). Considering $\overline{v^2}$ as an example, the volume-integrated production of $\overline{v^2}$ between the wall and the $P$-node may be approximated by (Hogg and Leschziner, 1989), i.e:

$$\int_{\Delta r}\int_{0}^{z_{\mathrm{p}}} P_{22}\,\mathrm{d}\forall \cong \int_{\Delta r}\int_{z_{\mathrm{v}}}^{z_{\mathrm{p}}} -2\overline{vw}\frac{\partial V}{\partial x}\,\mathrm{d}\forall = 2\tau_{\mathrm{w}}\left(\frac{V_{\mathrm{p}} - V_{\mathrm{v}}}{x_{\mathrm{p}} - x_{\mathrm{v}}}\right)x_{\mathrm{p}}\Delta r \tag{5}$$

where $V_{\mathrm{p}}$ and $V_{\mathrm{v}}$ follow from the log-law. No contribution arises from the viscous sublayer since $\overline{vw} = 0$ in this layer. An analogous integration of the dissipation rate with the assumptions,

$$\varepsilon = \frac{2\nu k_{\mathrm{v}}}{x_{\mathrm{v}}^2} \quad 0 \le x \le x_{\mathrm{v}}$$

$$\varepsilon = \frac{C_{\mu}^{3/4} k_{\mathrm{p}}^{3/2}}{\kappa x_{\mathrm{v}}} \quad x_{\mathrm{v}} \le x < x_{\mathrm{p}}$$

leads to

$$\int_{\Delta r}\int_{0}^{x_p} \varepsilon \, d\forall \cong \left[\frac{2\nu k_p}{x_v} + \frac{C_\mu^{3/4} k_p^{3/2}}{\kappa} \ln\left(\frac{x_p}{x_v}\right)\right] \Delta r \tag{6}$$

an analogous treatment is applied to $\bar{v^2}$, while the production of $\bar{w^2}$ in the viscous and turbulent near-wall layers region is zero (Versteeg and Malalasekera, 1995).

The values resulting from equations (5) and (6) are added, respectively, to the volume-integrated generation and dissipation computed for the upper half of the near-wall volume.

It should be noted that for the wall-law approach, the near-wall dissipation ($\varepsilon_p$) is not determined from its differential equation applied to the near-wall cell surrounding the node. Instead, and in accordance with the log-law, this value is obtained via the length scale from $\varepsilon_p = \left(C_\mu^{3/4} k_p^{3/2}\right)/(\kappa z_p)$, which serves as the boundary conditions for inner cells.

*Inlet conditions.* The boundary conditions for temperature and velocity need to be introduced at nozzle inlet:

$$T = \text{specified } (300\,\text{K}) \text{ and } U = \text{specified } (0.286\,\text{m/s})$$

The mass flow rate for the annular-conical and conical nozzles is kept the same.

The values of $k$ and $\varepsilon$ are not known at the inlet, but can be determined from turbulent kinetic energy, i.e.:

$$k = \lambda \bar{u}^2 \tag{7}$$

where $\bar{u}$ is the average inlet velocity and $\lambda$ is a percentage.

The dissipation is calculated from: $\varepsilon = C_\mu \left(k^{\frac{3}{2}}/aD\right)$, where $D$ is the diameter. The values $\lambda = 0.03$ and $a = 0.005$ are commonly used and may vary slightly in the literature (Elkaim *et al.*, 1992).

*Outlet.* The flow is considered to be extended over a long domain; therefore, the boundary condition (unbounded boundaries – Figure 2(a)) for any variable $\phi$ is:

$$\frac{\partial \phi}{\partial x_i} = 0 \tag{8}$$

where $x_i$ is the normal direction at outlet.

*Symmetry axis.* At the symmetry axis, the radial derivative of the variables is set to zero, i.e.:

$$\frac{\partial \phi}{\partial r} = 0 \tag{9}$$

except

$$V = \overline{vw} = \overline{vh} = \overline{wh} = 0$$

*2.2.1 Solid side. Constant temperature boundary.* Two constant temperature boundaries are considered. First one is in the radial direction far away from the symmetry axis constant temperature $T = T_{amb}$ (300 K) is defined (boundary A in Figure 2(a)). It should be noted that the constant temperature boundary condition is set at different locations in the radial directions at boundary A and no significant effect of

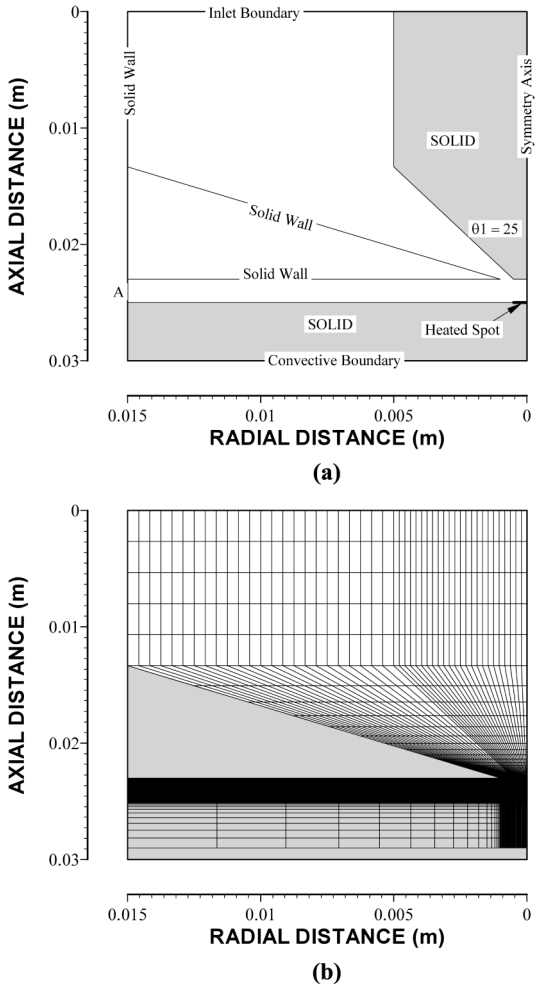


**Figure 2.**
View of (a) lay-out of the solution domain and boundary locations; and (b) grid used in the simulations

$T$ = constant was observed on the temperature and flow field in the stagnation region. Therefore, this boundary condition is set for radial distance 0.010 m from the symmetry axis. The second constant temperature boundary is set at the heated spot on the plate (as shown in Figure 2(a)) $T$ = constant (1,500 K).

*2.2.2 Solid fluid interface*. The coupling of conduction within the solid and convection within the fluid, termed conjugation, is required for the present analysis at the solid-fluid interface. The appropriate boundary conditions are continuity of heat flux and temperature and are termed boundary conditions of the fourth kind, i.e.:

$$T_{\mathrm{W_{solid}}} = T_{\mathrm{W_{gas}}}$$

$$K_{\mathrm{W_{solid}}} \frac{\partial T_{\mathrm{W_{solid}}}}{\partial x} = K_{\mathrm{W_{gas}}} \frac{\partial T_{\mathrm{W_{gas}}}}{\partial x}$$

No radiation losses from the solid surface is assumed due to the small size of the heated spot, which is in the order of 1 mm, and energy conducted into the solid to maintain the surface temperature at 1,500 K is considerably higher than the radiation losses from the surface (Shuja and Yilbas, 1998; Shuja *et al.*, 1998).

*2.3 Gas and solid properties*

The equation of state is used for air and the properties of gas and solid employed are given in Table II.

## 3. Numerical method and simulation

A control volume approach is employed when discretizing the governing equations. The discretization procedure is given in Patankar (1980). The problem of determining the pressure and satisfying continuity may be overcome by adjusting the pressure field so as to satisfy continuity. A staggered grid arrangement is used in which the velocities are stored at a location midway between the grid points, i.e. on the control volume faces. All other variables including pressure are calculated at the grid points. This arrangement gives a convenient way of handling the pressure linkages through the continuity equation and is known as Semi-Implicit Method for Pressure-Linked Equations (SIMPLE) algorithm. The details of this algorithm is given in Patankar (1980).

The computer program used for the present simulation can handle a non-uniform grid spacing. In each direction fine grid spacing near the gas jet impinging point and the hole is allocated while gradually increased spacing for locations away from the hole is considered. Elsewhere the grid spacing is adjusted to maintain a constant ratio of any of two adjacent spacings. The grid generated in the present study is shown in Figure 2(b). The number of grid planes used normal to the $r$ and $x$ directions are 64 and 134, respectively, thus making a total of 8,576 grid points. The grid independence tests were conducted and it was observed from Figure 3 that for $64 \times 134$ grid points, the predictions were in excellent agreement with the results of $80 \times 168$ grid points, i.e. the difference in predictions is about 0.1 per cent.

Six variables are computed at all grid points; these are: the two velocity components, the local pressure, the two turbulence quantities and the temperature.

## 4. Results and discussions

The influence of nozzle geometric configuration on flow and temperature fields due to jet impingement onto a flat surface with a limited heated area is investigated. Annular-conical and conical nozzles are considered to simulate the laser gas assisted conduction limited heating situation. In order to compare the effect of nozzle cone angles on the resulting velocity and temperature fields, the rate of mass flow passing

| Property | | Gas (air) | Solid (steel) |
|---|---|---|---|
| Density | $\rho$ (kg/m$^3$) | $p/RT$ | 8,030 |
| Thermal conductivity | $K$ (W/m K) | 0.0242 | 16.27 |
| Specific heat capacity | $c_p$ (J/kg K) | 1006.43 | 502.48 |
| Viscosity | $\nu$ (kg/m s) | $1.7894 \times 10^{-5}$ | |

**Table II.** Properties used in the simulation

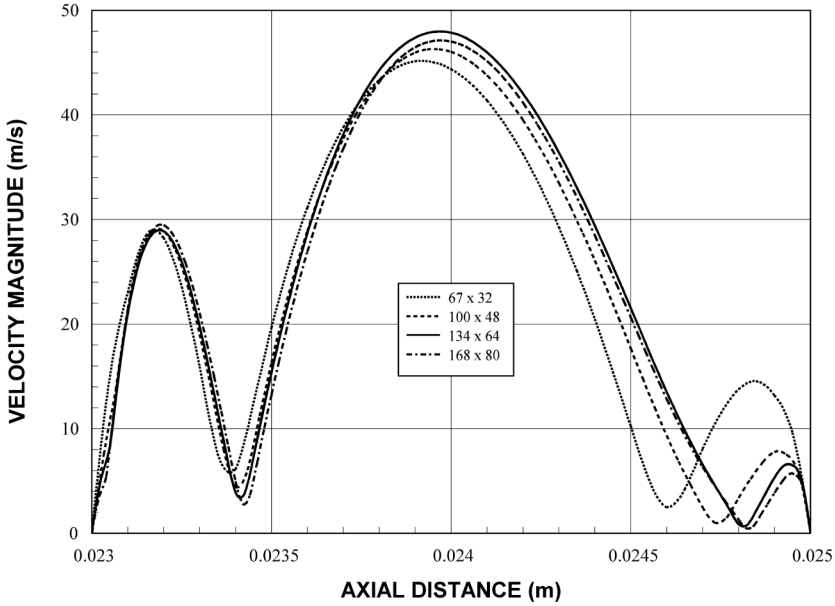


**Figure 3.**
The results of grid independence tests (radial location is the symmetry axis)

through the nozzles with different cone angles are kept constant while the cone angle of annular-conical and conical nozzles is varied. The limited area of the substrate surface, resembling the laser irradiated spot at the surface, is kept at 1,500 K. In addition, fully developed jet exit conditions are also accommodated for the comparison purpose.

Figure 4 shows velocity magnitude contours for annular-conical nozzle for different cone angles. Since, the flow situation is axisymmetric, half of the solution domain is presented in the figure. The expansion of the jet accelerates the flow in the region next to the nozzle exit. The exit velocity profile of annular nozzle varies with changing nozzle cone angle. This can also be seen from Figure 5, in which nozzle exit velocity profiles are shown. In general, the nozzle exit profiles are similar to the annular flow velocity profiles, i.e. the magnitude of velocity is higher close to the nozzle outer edge. The nozzle exit velocity profiles corresponding to different nozzle cone angles appear to be similar, provided their magnitude changes, i.e. large cone angles result in high velocity magnitude in the region close to the outer edge. It should be noted that the influence of flat plate spacing on nozzle exit velocity profiles is tested by extending the plate spacing (nozzle exit-to-plate spacing) five times the original spacing. It is observed from Figure 5 that the plate spacing has not any influence on the nozzle exit velocity profiles. Moreover, due to the stagnation region developed close to the solid wall the jet bends radially, which in turn enhances the radial flow particularly in the region close to the solid wall and next to the stagnation region. This is more pronounced as the nozzle cone angle increases ($\theta = 40°$). Owing to oblique impingement due to annular nozzle, the complex flow structure is developed close to the solid wall (Simon *et al.*, 1993). In this case, the radial expansion of the jet is highly influenced by the cone angle of the annular nozzle. Moreover, the behaviour of radial expansion results in a radial jet similar to the confined wall jets (Witze and Dwyer,

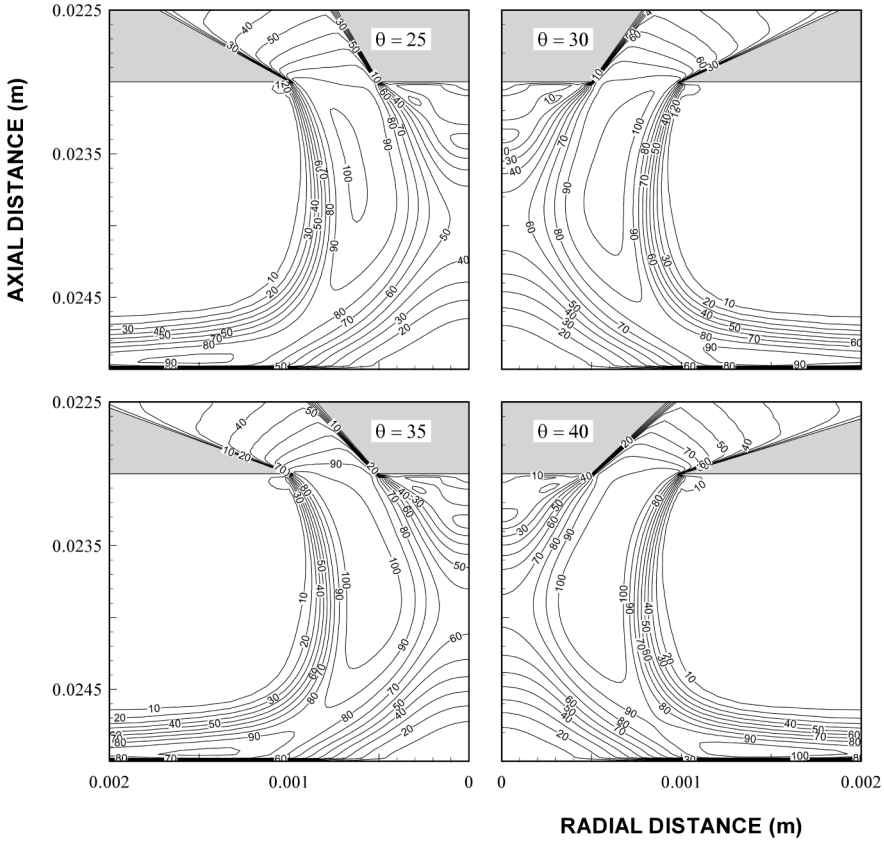


**Figure 4.**
Velocity magnitude contours in the region close to the heated spot for different inner cone angles (angles are in degrees)

1976), provided that radial jet expansion differs for different annular nozzle cone angles.

Figure 6 shows the pressure contours for annular-conical nozzles for different cone angles. The stagnation region close to the solid wall extends into the impinging jet side as cone angle of the nozzle increases. This is because of the high oblique angle of the impinging jet; in this case, jet bends more towards radially under the influence of the stagnation zone and it expands radially resulting in reduced pressure next to the stagnation zone. In this case, the size of stream line curvature corresponding to relatively low pressure ($\sim$1 kPa) becomes slightly larger for large cone angle nozzles. The extension of stagnation region into upstream flow is also evident form Figure 7, in which pressure coefficient along the $z$-axis at different radial location is shown. It should be noted that the reverse flow developed in the region close to the flat plate surface influences the size of the stagnation zone. Consequently, as the reverse flow, which enhances with increasing nozzle cone angle, increases the stagnation region extends away from the solid wall.

Figure 8 shows the velocity magnitude along the symmetry axis for different annular nozzle cone angles. The conical oblique expansion of the annular jet results in a complex flow structure close to the solid wall. In this case, reverse flow occurs in the

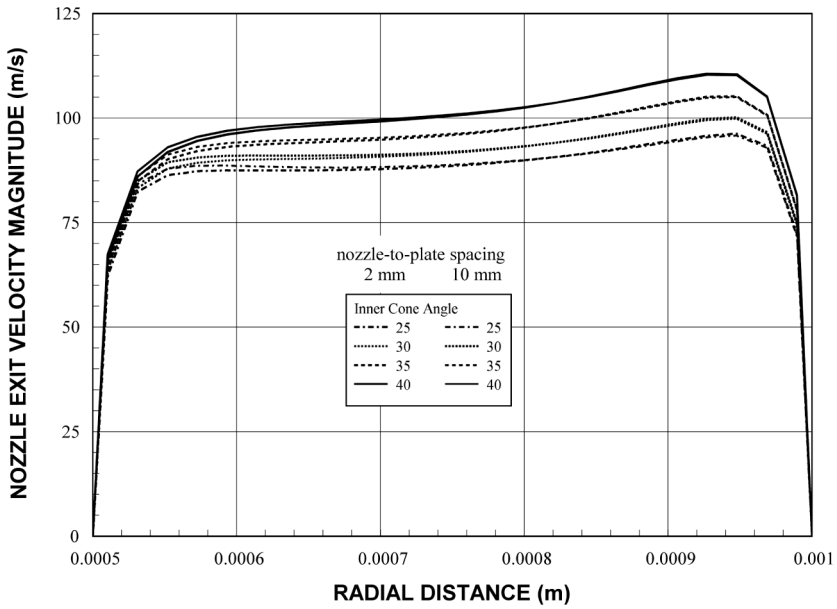


**Figure 5.**
The variation of velocity magnitude at the exit of the nozzle for two nozzle-to-plate spacing and different annular-nozzle inner cone angles

region close to the wall. This occurs because of the non-symmetric velocity profile exiting the nozzle; consequently, the shear flow close to the stagnation region generates an adverse pressure gradient in this region. Furthermore, the radial expansion of the jet enhances the shear flow in this region. When examining the pressure coefficient along the axial direction at different radial locations (Figure 7), the stagnation region extends away from the surface as the nozzle cone angle increases. The reverse flow in between the solid wall and stagnation zone is also evident. Moreover, radial extension of the reverse flow is suppressed by the jet stream line curvature effect. Therefore, as cone angle increases, the size of the reverse flow in the radial direction increases slightly.

Figure 8 shows heat transfer coefficient along the radial direction for two nozzle types (annular-conical and conical nozzles) and different nozzle cone angles. It should be noted that heat transfer coefficient corresponding to fully developed jet exiting velocity profile is also included for the comparison purposes. The jet exit velocity profile identical to fully developed pipe flow velocity profile results in highest heat transfer coefficient across the heated spot. This occurs because of the stagnation zone in the region close to the wall; in this case, sharp decay of velocity magnitude close to the solid wall results in enhanced radial flow in this region. Consequently, convective cooling of the surface improves significantly. Moreover, the complex flow structure such as fluid mixing in the stagnation region enhances the convective cooling of the solid surface. The complex flow structure is also evident from velocity magnitude curve (Figure 8), i.e. velocity magnitude first reduces and then increases in this region. The annular-conical nozzles result in higher heat transfer coefficients as compared to that corresponding to conical nozzles, despite the fact that the mass flow rate and mean velocity exiting the nozzle are the same for both nozzles. Heat transfer improvement across the heated spot for annular-conical nozzle is due to flow mixing in the stagnation region and enhancement of radial flow. In this case, the nozzle with high

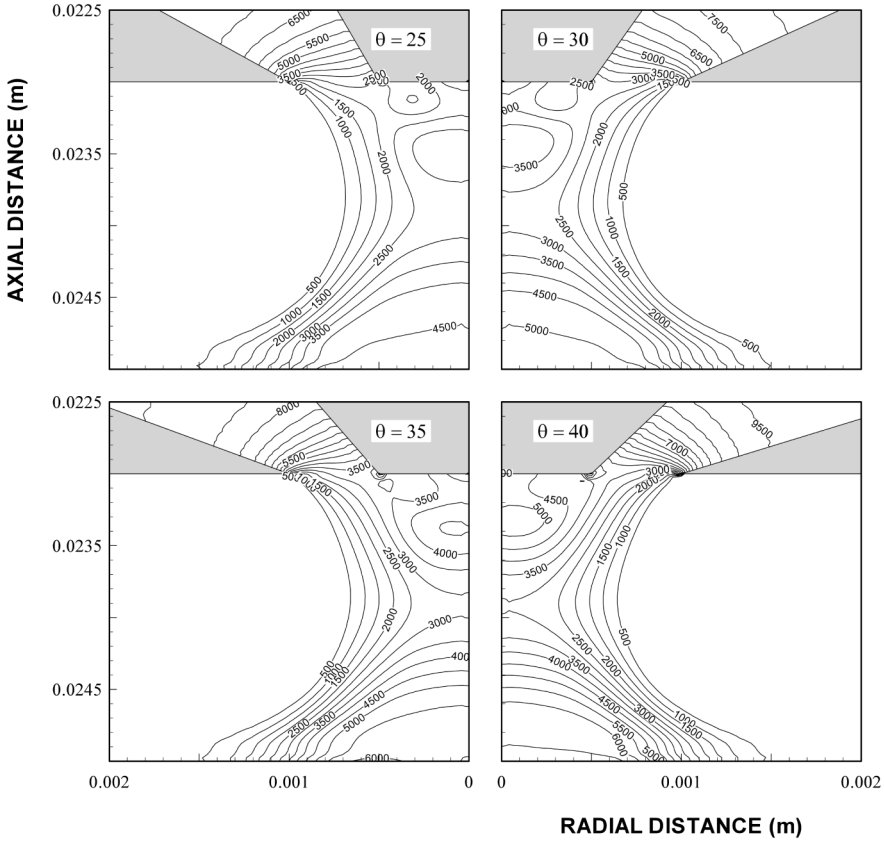


**Figure 6.**
Pressure contours in the region close to the heated spot for different inner cone angles (angles are in degrees)

cone angle improves the heat transfer coefficient. In the case of conical nozzles, heat transfer coefficient reduce almost 20 per cent of that annular nozzles. It should be noted that the nozzle exit velocity profile of conical nozzles differs significantly from the annular-conical nozzles. This indicates that although both mass flow rate, mean nozzle exit velocity and cross-sectional area are the same for both nozzles, onset of different nozzle exiting velocity profiles influences the heat transfer coefficient significantly. In laser gas assisted machining applications, fully developed pipe flow velocity profile cannot be achieved at the nozzle exit. However, in practical applications either conical or annular-conical nozzles are used. Consequently, in laser gas assisted conduction limited heating situation, to achieve high cooling rates of the surface, the annular-conical nozzles have considerable advantages over the conical nozzles.

## 5. Conclusions

Jet impingement onto a limited area heated flat plate is considered in relation to laser gas assisted processing. The influence of nozzle geometric configurations on the flow field and heat transfer characteristics are examined. In this case, annular-conical and

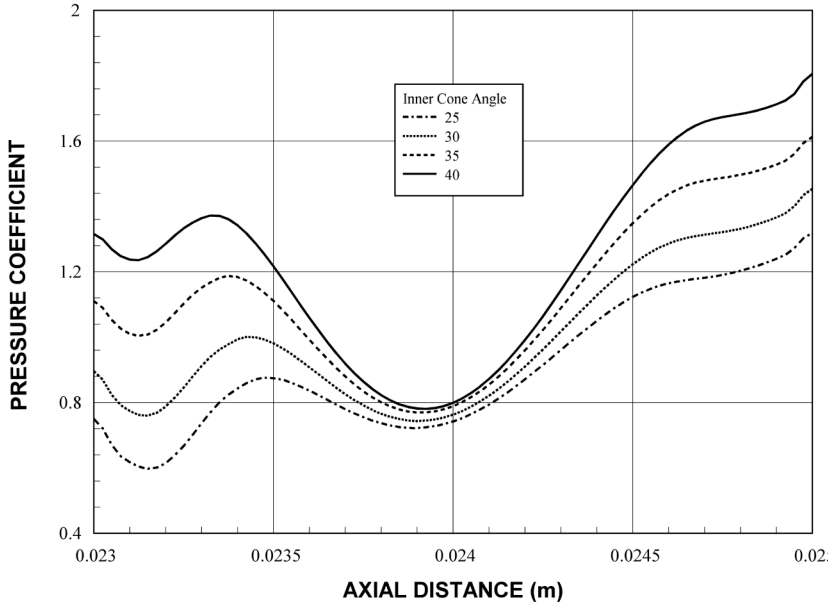


**Figure 7.**
The pressure coefficient distribution along the symmetry axis for different annular nozzle inner cone angles

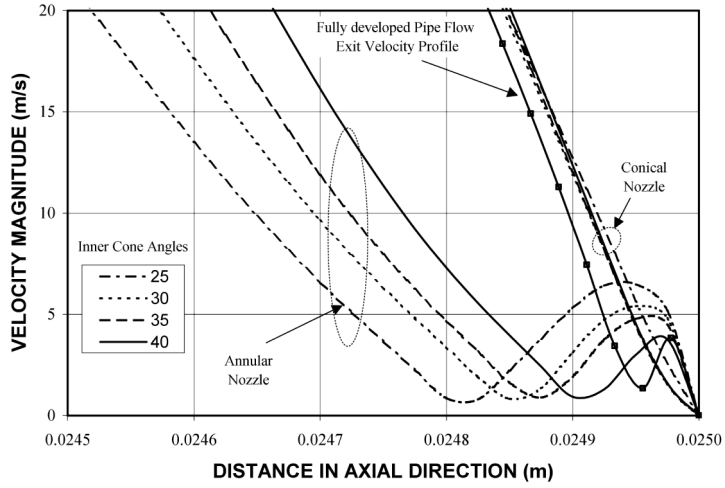


**Figure 8.**
Velocity magnitude along the symmetry axis for two nozzles and fully developed pipe flow. The nozzle inner cone angles are varied

conical nozzles are selected due to their wide usage in laser machining applications. In order to compare heat transfer coefficients corresponding to different nozzle configurations, a velocity profile for fully developed pipe flow as impinging onto a plate is also accommodated. It is found that nozzle exiting velocity profiles differ considerably with changing the nozzle cone angle. This, in turn, results in different flow structure close to the flat plate surface. In this case, increasing nozzle cone angle

enhances the radial flow and extends the stagnation zone away from the plate surface. This situation is observed particularly for the annular-conical nozzles. The impinging jet with a fully developed velocity profile results in enhanced radial acceleration of the flow as observed in the previous studies. Moreover, the flow structure changes considerably for annular conical and conical nozzles. This in turn alters the heat transfer coefficient within an order of 20 per cent as compared to conical nozzles for the same mass flow rate and nozzle exiting mean velocity. This is because of the flow mixing in the region close to the stagnation zone and enhancement of radial flow in this region, i.e. annular-conical nozzle enhances the radial flow in the region next to the stagnation zone. Moreover, nozzle exiting velocity profile which is identical to fully developed pipe flow velocity profile results in improved heat transfer coefficient at the flat plate surface. However, the achievement of fully developed pipe flow like velocity profile emanating a nozzle is almost impossible for practical laser applications. Consequently, annular-conical nozzles have advantage over conical nozzles due to high heat transfer coefficients. Therefore, use of annular-conical nozzles facilitate the high cooling rates from the surface during laser heating process.

## References

Baughn, J.W. and Shimizu, S. (1989), "Heat transfer measurements from a surface with uniform heat flux and an impinging jet", *ASME Journal of Heat Transfer*, Vol. 111, pp. 1096-8.

Benocci, C. (1991), *Introduction to the Modeling of Turbulence, 1991-2002*, Von Karman Institute for Fluid Dynamics, March.

Cooper, D., Jackson, D.C., Launder, B.E. and Liao, G.X. (1993), "Impinging jet studies for turbulence model assessment – i. Flow-field experiments", *International Journal of Heat and Mass Transfer*, Vol. 36 No. 36, pp. 2675-84.

Neto, O.D. and Lima, C.A.S. (1994), "Nonlinear three-dimensional temperature profiles in pulsed laser heated solids", *Journal of Physics D, Transactions in Applied Physics*, Vol. 27, pp. 1795-804.

Elison, B. and Webb, B.W. (1994), "Local heat transfer to impinging liquid jets in the initially laminar, transitional, and turbulent regimes", *International Journal of Heat and Mass Transfer*, Vol. 37 No. 8, pp. 1207-16.

Elkaim, D., Reggio, M. and Camarero, R. (1992), "Simulating two-dimensional turbulent flow by using the $k$-$\varepsilon$ model and the vorticity-stream function formulation", *International Journal for Numerical methods in Fluids*, Vol. 14, pp. 961-80.

Garimella, S.V. and Rice, R.A. (1995), "Confined and submerged liquid jet impingement heat transfer", *ASME Journal of Heat Transfer*, Vol. 117, pp. 871-7.

Hector, L.G. Jr, Kim, W.S. and Ozisik, M.N. (1992), "Hyperbolic heat conduction due to a mode locked laser pulse train", *International Journal of Engineering Sciences*, Vol. 30 No. 2, pp. 1731-44.

Hogg, S. and Leschziner, M.A. (1989), "Second-moment-closure calculation of strongly swirling confined flow with large density gradients", *International Journal of Heat and Fluid Flow*, Vol. 10 No. 1, pp. 16-27.

Huang, L. and El-Genk, M.S. (1994), "Heat transfer of an impinging jet on a flat surface", *International Journal of Heat and Mass Transfer*, Vol. 37 No. 13, pp. 1915-23.

Launder, B.E. (1989), "Second-moment closure and its use in modelling turbulent industrial flows", *International Journal for Numerical Methods in Fluids*, Vol. 9, pp. 963-85.

Lee, D., Greif, R., Lee, S.J. and Lee, J.H. (1995), "Heat transfer from a flat plate to a fully developed axisymmetric impinging jet", *ASME Journal of Heat Transfer*, Vol. 117, pp. 772-6.

Mohanty, A.K. and Tawfek, A.A. (1993), "Heat transfer due to a round jet impinging normal to a flat surface", *International Journal of Heat and Mass Transfer*, Vol. 36 No. 6, pp. 1639-47.

Morris, G.K., Garimella, S.V. and Amano, R.S. (1996), "Prediction of jet impingement heat transfer using a hybrid wall treatment with different turbulent prandtl number functions", *ASME Journal of Heat Transfer*, Vol. 118, pp. 562-9.

Patankar, S.V. (1980), *Numerical Heat Transfer*, McGraw-Hill, New York, NY.

Shuja, S.Z. and Yilbas, B.S. (1998), "Gas assisted laser repetitive pulsed heating of steel surface", *Proceedings of IMechE, Part C: Journal of Mechanical Sciences*, Vol. 212, pp. 741-57.

Shuja, S.Z., Yilbas, B.S. and Budair, M.O. (1998), "Modeling of laser heating of solid substance including assisting gas impingement", *Numerical Heat Transfer, Part A*, Vol. 33, pp. 315-39.

Shuja, S.Z., Yilbas, B.S. and Budair, M.O. (1999), "Gas jet impingement on a surface having a limited constant heat flux area: Various turbulence models", *Numerical Heat Transfer: Part A*, (in press).

Simon, G., Gratzke, U. and Kroos, J. (1993), "Analysis of heat conduction in deep penetration welding with a time-modulated laser pulse", *Journal of Physics D, Transactions in Applied Physics*, Vol. 26, pp. 862-9.

Stevens, J., Pan, Y. and Webb, B.W. (1992a), "Effect of nozzle configuration on transport in the stagnation zone of axisymmetric, impinging free-surface liquid jets: Part 1 – turbulent flow structure", *ASME Journal of Heat Transfer*, Vol. 114, pp. 874-9.

Stevens, J., Pan, Y. and Webb, B.W. (1992b), "Effect of nozzle configuration on transport in the stagnation zone of axisymmetric, impinging free-surface liquid jets: Part 2 – local heat transfer", *ASME Journal of Heat Transfer*, Vol. 114, pp. 880-6.

Versteeg, H.K. and Malalasekera, W. (1995), *An Introduction to Computational Fluid Dynamics, The Finite Volume Method*, Longman Scientific and Techinical, New York, NY.

Witze, P.O. and Dwyer, H.A. (1976), "The turbulent radial jet", *Journal of Fluid Mechanics*, Vol. 75, pp. 401-17.

Wolf, D.H., Viskanta, R. and Incropera, F.P. (1995a), "Turbulence dissipation in a free-surface jet of water and its effects on local impingement heat transfer from a heated surface: Part 1 – flow structure", *ASME Journal of Heat Transfer*, Vol. 117, pp. 85-94.

Wolf, D.H., Viskanta, R. and Incropera, F.P. (1995b), "Turbulence dissipation in a free-surface jet of water and its effects on local impingement heat transfer from a heated surface: Part 2 – local heat transfer", *ASME Journal of Heat Transfer*, Vol. 117, pp. 95-103.

Yilbas, B.S. (1997), "Analytical solution for time unsteady laser pulse heating of semi-infinite solid", *International Journal of Mechanical Sciences*, Vol. 39 No. 6, pp. 671-82.

Yilbas, B.S. and Shuja, S.Z. (1997), "Heat transfer analysis of laser heated surfaces-conduction limited case", *Applied Surface Science*, Vol. 108, pp. 167-75.

Yilbas, B.S., Shuja, S.Z. and Budair, M.O. (2000), "Nano-second pulse heating and gas assisting jet considerations", *International Journal of Machine Tools and Manufacture*, Vol. 40, pp. 1023-38.

Yilbas, B.S., Shuja, S.Z. and Budair, M.O. (2002), "Stagnation point flow over a heating plate: Consideration of gas jet velocity profiles", *The Arabian Journal for Science and Engineering*, Vol. 27, pp. 91-116.